

Analyzing power and transversity cross sections for π^+p and π^-p elastic scattering from 471 to 687 MeV/c

A. Mokhtari,* A. D. Eichon,[†] G. J. Kim, B. M. K. Nefkens, and J. A. Wightman
Department of Physics, University of California, Los Angeles, California 90024

D. H. Fitzgerald

*Department of Physics, University of California, Los Angeles, California 90024
and Los Alamos National Laboratory, Los Alamos, New Mexico 87545[‡]*

W. J. Briscoe

*Department of Physics, University of California, Los Angeles, California 90024
and Department of Physics, George Washington University, Washington, D.C. 20052[‡]*

M. E. Sadler

*Department of Physics, Abilene Christian University, Abilene, Texas 77699
(Received 12 May 1986)*

We have obtained precise data on the analyzing power for π^+p and π^-p elastic scattering at 471, 547, 625, and 687 MeV/c using a transversely polarized target. Using our previously measured differential cross sections at the above beam momenta, we have determined the transversity cross sections and the bounds of the isospin triangle inequalities. Comparisons are made with the results of existing partial wave analyses by the Karlsruhe-Helsinki, Carnegie-Mellon University-LBL, and VPI groups. The π^+ predictions are in acceptable agreement with our data, while the agreement is less acceptable for π^- .

I. INTRODUCTION

The pion-nucleon system exhibits many resonances below 3 GeV (Ref. 1). These may be interpreted as excited states of the nucleon or as different three-quark configurations. The very existence of nearly all πN resonances as well as their characteristics, such as mass and width, have been deduced using partial-wave analyses of the differential cross sections and analyzing powers of πN elastic and charge-exchange (CEX) scattering. Because the existing data sets are incomplete they do not uniquely determine the partial wave amplitudes.² The problem of the unambiguous determination of the πN amplitudes is especially complicated in energy regions where two or more resonances overlap significantly.

We report precise measurements of the analyzing power A_N for π^+p and π^-p elastic scattering at four incident pion momenta: 471, 547, 625, and 687 MeV/c (center-of-mass energies from 1350 to 1490 MeV). The A_N values have been determined over a wide range of scattering angles ($-0.9 \leq \cos\theta_{c.m.} \leq 0.5$) by measuring elastic scattering from a transversely polarized target. This article is the detailed account of our experiment, which was reported earlier in preliminary form.^{3,4} The experiment is part of our program for measuring the complete set of observables ($d\sigma/d\Omega$, A_N , A , and R) for πp elastic and CEX scattering at several momenta. The differential-cross-section data for elastic scattering at these beam momenta have been previously reported.⁵

In addition to supplying accurate data on the π^+p and π^-p systems for the determination of the isospin $I = \frac{1}{2}$ and $\frac{3}{2}$ scattering amplitudes, the measurements contribute

to progress on several issues of current interest. The search for new low-mass resonances is a help in testing a variety of quark models.⁶⁻¹⁵ Accurate πN amplitudes are important for the construction of improved nucleon-nucleon potentials based on meson exchange and for π -nucleus potentials.¹⁶ Accurate experimental data are needed to test recent πN phase-shift predictions based on the Skyrme-soliton¹⁷⁻²² and the $\pi\Delta$ -coupling models.²³

II. PARTIAL-WAVE ANALYSIS

The determination of the complete and unambiguous set of πN amplitudes requires a measurement of four independent observables (at each energy and angle), the differential cross section $d\sigma/d\Omega$, the analyzing power A_N , and the Wolfenstein spin-rotation parameters A and R . As no measurement has yet been made of A and R below 6 GeV/c, the ambiguities in πN partial-wave analyses (PWA's) that are a consequence of the use of an incomplete data set are resolved using theoretical constraints. These constraints typically include unitarity, analyticity (via dispersion relations) and isospin invariance. Various groups have obtained πN scattering amplitudes by fitting the measured cross sections and analyzing powers for πp elastic and CEX scattering, making varying uses of theoretical constraints. There are three recent partial-wave analyses available from the Karlsruhe-Helsinki²⁴ (KH) group, the Carnegie-Mellon University-Lawrence Berkeley Laboratory²⁵ (CMU-LBL) Collaboration, and the Virginia Polytechnic Institute and State University²⁶ (VPI) group. The difference among these PWA's lies in the application of theoretical constraints and in the data-

base. The KH and CMU-LBL analyses rely on the use of dispersion relations, while the VPI analysis relies almost exclusively on experimental input. The PWA's differ in the number of resonances obtained as well as in their mass and width. For example, evidence for a new P_{33} resonance has been seen, but inconsistent values are reported for its mass. KH (Ref. 24) gives 1522 ± 13 MeV, while CMU-LBL (Ref. 25) reports 1600 ± 50 MeV. The Roper resonance $N(1440)P_{11}$ is another example. There is uncertainty over its properties that fuels controversies regarding its structure and the quark-model classification. The PWA's do not concur on the mass M , or the width Γ , or the elasticity η . KH reports $M = 1410 \pm 12$ MeV, $\Gamma = 135 \pm 10$ MeV, and $\eta = 0.51 \pm 0.05$, while the CMU-LBL Collaboration quotes $M = 1440 \pm 30$ MeV, $\Gamma = 340 \pm 70$ MeV, and $\eta = 0.68 \pm 0.04$. The controversy over the width is particularly interesting because there is a possibility that there could be two closely spaced P_{11} resonances. Ayed²⁷ first proposed a split of the Roper resonance based on the Saclay PWA; he found masses of 1413 and 1532 MeV. Although this proposed split is not seen in the KH or CMU-LBL analyses, the latest PWA by the VPI (Ref. 26) group, which characterizes the resonances in terms of the pole positions in the complex energy plane rather than the Breit-Wigner parametrization, shows two P_{11} poles: $P_{11}(I) = (1359 - 100i)$ MeV and $P_{11}(II) = (1410 - 80i)$ MeV.

III. MODELS

There are many quark models that account for the spectra of baryons, notably, the bag⁶⁻¹⁰ and potential models.^{11,12} Furthermore, there are some exciting speculations concerning the existence of a new state of matter consisting of three quarks and a gluon, called hybrid matter.¹³⁻¹⁵ Recently, explicit calculations of the phase shifts have been made in the context of the Skyrme soliton model.¹⁷⁻²² Also, it has been argued that some resonances seen in πN elastic scattering, including the Roper resonance, may actually be due to the opening of the threshold for the production of the $\Delta(1232)$ (Ref. 23). The ultimate test of a successful model for baryon structure is a comparison with the experimentally determined spectra of the baryon resonances. Our measurements reflect on the properties of the P_{11} resonance. In order to illustrate the diversity of theoretical treatments of the baryon structures, we mention briefly a variety of models that make predictions for the P_{11} phase in the energy region of the Roper resonance.

A. Bag model

The difficulties encountered in solving the equations of quantum chromodynamics (QCD) have given rise to quark models which incorporate some of the features of QCD phenomenologically. One way of handling confinement is to regard the quarks and gluons as contained in a rigid spherical cavity or bag.⁶

The Roper resonance is a strong candidate for a radial excitation of the nucleon, i.e., it is thought to have a $(1S)^2(2S)$ configuration of three quarks [i.e., with two

quarks in the ground state ($1S$) and one quark excited to a ($2S$) cavity eigenmode]. DeGrand and Rebbi⁷ have investigated the lowest radially excited states of the bag model. Breathing excitations of the surface of the bag couple to the radially excited states of quarks in the bag, resulting in a spectrum of states which lie between the energy levels of the fixed-cavity approximation. In their model the Roper resonance has a mass of 1410 MeV and a second P_{11} state occurs at 1603 MeV.

The properties of the P_{11} resonances in the context of the cloudy bag model have been evaluated by Umland *et al.*⁸ These authors predict a doublet of states with masses of 1418 and 1533 MeV. Bowler and Hey⁹ have studied radially excited baryon states in the framework of the MIT bag model.⁶ They stress the importance of the direct gluon-exchange contribution and obtain physical P_{11} states of 1543 and 1646 MeV. Close and Horgan¹⁰ have included an exchange amplitude and the surface oscillation term of DeGrand and Rebbi⁷ in the direct gluon-exchange model of Bowler and Hey⁹ and predict P_{11} masses of 1416 and 1617 MeV.

B. Potential models

Nonrelativistic potential models for mesons and baryons based on one-gluon exchange date back to the 1975 paper by De Rújula, Georgi, and Glashow¹¹ (DRGG), in which the quark model is interpreted within the framework of quark dynamics described by QCD. The essential feature of the model is the inclusion of a one-gluon-exchange interaction to account for the interquark interaction at short distances. Since the appearance of the DRGG model, many authors have predicted the existence and parameters of N^* states using confining potentials based on a variety of two-body potentials. Karl, Isgur, and Koniuk¹² (KIK) use an anharmonic-oscillator Hamiltonian perturbation and a hyperfine correction. The key to the successful phenomenology of this model is the neglect of the spin-orbit force and retention of the spin-spin interaction. The KIK quark model has no room for the $P_{31}(1550)$, a one-star candidate seen in pion photoproduction and in $\pi N \rightarrow \pi\pi N$. There is also an experimental two-star P_{33} candidate with a mass of either 1522 MeV (KH) or 1600 MeV (CMU-LBL), whereas the KIK quark model predicts a P_{33} with a mass of about 1780 MeV. The model also predicts two P_{11} resonances at 1405 and 1705 MeV.

C. Hybrid states

In the last two decades several empirical descriptions of hadrons have emerged which include the existence of hadrons that are constructed from constituent quarks or constituent gluons. Thus, hybrid configurations containing some of each should also exist.^{13,14} The lowest-mass hybrid baryon candidate is a P_{11} state with a mass near 1500 MeV (Refs. 13 and 15). It is interesting to speculate that the reported splitting of the Roper resonance might be a manifestation of the existence of a hybrid P_{11} in addition to the ordinary three-quark P_{11} resonance.

D. Skyrme soliton models

Recently, pion-nucleon phase shifts have been calculated in the context of the Skyrme soliton model. Based on this model new baryon resonances have been predicted¹⁷ and novel relations among isospin- $\frac{1}{2}$ and $-\frac{3}{2}$ waves have been established.¹⁸ The Skyrme model is a low-energy effective Lagrangian. Using the experimental value for the elasticity of the P_{11} channel, Hayashi *et al.*¹⁹ find that the P_{11} resonance should occur 50–100 MeV below the experimental Roper resonance. Liu *et al.*²⁰ have addressed dynamical aspects of the Skyrme soliton through its time dependence. Their Roper resonance mass is lower than the experimental value by about 200 MeV. Breit and Nappi²¹ have studied the simplest vibrational excitation of the skyrmion, the breathing mode. Only for a pion mass of about 300–400 MeV does their P_{11} resonance look like the experimental one. For a pion mass of 140 MeV there is a resonance, but the phase shifts reach a maximum of only about 91° instead of 180° . They identify the Roper resonance with a nucleon breathing mode at 1270 MeV. In the chiral limit the phase shifts reach a maximum which is less than 90° . This has led Zahed *et al.*²² to conclude that there is no resonance in this channel.

E. $\pi\Delta$ coupling model

Starting from a point of view that is opposite to the preceding models, Blankleider and Walker²³ have investigated the possibility that certain πN resonances may be a manifestation of coupling in the $\pi\Delta(1232)$ channel and that some of the low-lying resonances seen in πN elastic scattering may be due to the opening of the threshold for $\pi\Delta$ production. In view of the limitations of the one-pion-exchange approximation at high energies, they have restricted their discussion to pion laboratory energies below 1 GeV. They find excellent fits to the P_{11} , D_{13} , D_{15} , and S_{31} phase shifts and inelasticities without the need for introducing the established four-star $P_{11}(1440)$, $D_{13}(1520)$, $D_{15}(1675)$, and $s_{31}(1620)$ resonances explicitly. They do not claim that there is no need for true particle resonances, since the mechanism of coupling to the $\pi\Delta$ channels can also give rise to resonance behavior.

IV. πN SCATTERING FORMALISM

The differential cross section for scattering from a target with polarization \mathbf{P}_T is

$$I(\theta, \phi) = I_0(\theta) [1 + A_N(\theta) \mathbf{P}_T \cdot \hat{\mathbf{n}}], \quad (1)$$

where $A_N(\theta)$ is the analyzing power of the reaction, and $\hat{\mathbf{n}}$ is the unit vector normal to the scattering plane. For a transversely polarized target, \mathbf{P}_T is either parallel or antiparallel to $\hat{\mathbf{n}}$. When \mathbf{P}_T is parallel to $\hat{\mathbf{n}}$ we have

$$I_+ = I_0(1 + A_N P_T). \quad (2)$$

With $p_T = 1$, I_+ is the parallel transversity cross section. When \mathbf{P}_T and $\hat{\mathbf{n}}$ are antiparallel we have

$$I_- = I_0(1 - A_N P_T). \quad (3)$$

With $P_T = 1$, I_- is the antiparallel transversity cross section. The asymmetry parameter $\epsilon(\theta)$ is defined as

$$\epsilon(\theta) = \frac{I_+ - I_-}{I_+ + I_-}, \quad (4)$$

where

$$A_N(\theta) = \frac{\epsilon(\theta)}{P_T}. \quad (5)$$

Only the asymmetry and the target polarization need be measured to obtain the analyzing power; only relative measurements of I_+ and I_- are required.

The $\pi^\pm p$ elastic and CEX scattering amplitudes a^\pm and a^0 are related through isospin invariance. The three amplitudes describing scattering from a transversely polarized target are

$$I_\pm^+ = \frac{d\sigma}{d\Omega}(\pi^+ p \rightarrow \pi^+ p) = |a_\pm^+|^2, \quad (6a)$$

$$I_\pm^- = \frac{d\sigma}{d\Omega}(\pi^- p \rightarrow \pi^- p) = |a_\pm^-|^2, \quad (6b)$$

and

$$I_\pm^0 = \frac{d\sigma}{d\Omega}(\pi^- p \rightarrow \pi^0 n) = |a_\pm^0|^2. \quad (6c)$$

The subscripts (\pm) refer to parallel and antiparallel transversity cross sections defined in Eqs. (2) and (3). The superscripts $+$, $-$, and 0 refer to $\pi^\pm p$ elastic and $\pi^- p$ charge-exchange scattering. Isospin invariance implies only two independent isospin amplitudes, $a_{1/2}$ and $a_{3/2}$.

$$a^+ = a_{3/2}, \quad (7a)$$

$$a^- = \frac{1}{3}(a_{3/2} + 2a_{1/2}), \quad (7b)$$

and

$$a^0 = \frac{\sqrt{2}}{3}(a_{3/2} - a_{1/2}). \quad (7c)$$

The transversity subscripts are suppressed. Therefore, isospin invariance requires

$$a^+ = a^- + \sqrt{2}a^0, \quad (8)$$

i.e., the amplitudes form a triangle in the complex plane. Thus,

$$|a^+| - |a^-| \leq \sqrt{2}|a^0| \leq |a^+| + |a^-|. \quad (9)$$

For parallel transversity cross sections we find

$$\frac{1}{2}(\sqrt{I_+^+} - \sqrt{I_+^-})^2 \leq I_+^0 \leq \frac{1}{2}(\sqrt{I_+^+} + \sqrt{I_+^-})^2, \quad (10)$$

and for antiparallel transversity cross sections

$$\frac{1}{2}(\sqrt{I_-^+} - \sqrt{I_-^-})^2 \leq I_-^0 \leq \frac{1}{2}(\sqrt{I_-^+} + \sqrt{I_-^-})^2. \quad (11)$$

A similar triangle inequality holds for unpolarized differential cross sections. Only analyzing powers and unpolarized differential cross sections for elastic and CEX scattering are needed to test triangle inequalities (10) and (11).

V. EXPERIMENT

The experiment was carried out at the Clinton P. Anderson Meson Physics Facility (LAMPF) in the east cave

of the Pion Particle Physics (P^3) channel. The design and performance of the channel are described in detail elsewhere.²⁸ The experimental setup is shown in Fig. 1. A π^+ or π^- beam was incident on a transversely polarized proton target. The scattered pions were detected in a magnetic spectrometer and the recoil protons in a detector consisting of a wire chamber and two scintillator hodoscopes.

A. Pion beams

The characteristics of the π^+ and π^- beams are given in Table I. The central beam momentum is determined by the first bending magnet in the channel and is known to $\pm 0.3\%$ (Refs. 29 and 30). The calculation of the average momentum in the target includes the ionization energy loss in the vacuum windows, a short air path, and in all materials comprising the polarized target. The channel momentum acceptance is defined by a set of jaws at a high dispersion point in the channel. A small steering magnet at the end of the P^3 channel was used to compensate for the horizontal deflection of the beam in the field of the polarized target magnet. The transverse-spot size and position of the beam were monitored using two beam-profile monitors, BPM 1 and BPM 2, located upstream of the target. These BPM's were used to determine the final steering and focusing of the beam; during data taking the BPM's were used to verify that the beam position and spot size remained constant within the BPM resolution (2 mm). The beam spot at the target was approximately 2 cm in diameter, as measured with Polaroid film. The beam divergence was typically 10 msr. Relative beam intensities were measured using two plastic-

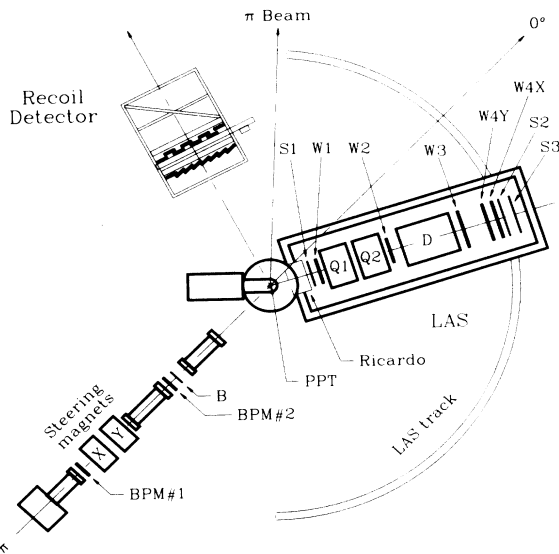


FIG. 1. Layout of the experimental setup. BPM 1 and BPM 2 are the beam-profile monitors; B is the beam counter hodoscope. $S1-S3$ represent the LAS entrance and exit scintillation counters; $W1-W4$ are the LAS multiwire proportional chambers. The LAS quadrupoles are marked $Q1$ and $Q2$ and D is the bending dipole magnet. Also shown are the polarized-proton target (PPT) and the Ricardo steering magnet.

TABLE I. Beam characteristics.

| Average momentum in the target (MeV/ c) | Beam polarity | $\Delta p/p^a$ (%) | Deflection in PPT (deg) |
|--|------------------|-----------------------|-------------------------------|
| 470.8 | π^+ | 2.0 | 18.1 |
| 470.8 | π^- | 4.7 ^b | 18.1 |
| 546.9 | π^+ | 0.5 | 15.5 |
| 546.9 | π^- | 0.8 | 15.5 |
| 624.9 | π^+ | 2.0 | 13.5 |
| 624.9 | π^- | 3.3 | 13.5 |
| 687.0 | π^+ | 5.3 ^c | 12.3 |
| 687.0 | π^- | 2.7 ^d | 12.3 |

^aFull width at half maximum.

^bMomentum slits were set asymmetrically.

^cSome data were taken with a momentum bite of 2.7% and some with even smaller $\Delta p/p$.

^dThe data of $\theta_{c.m.} = 140^\circ$ and part of the data at $\theta_{c.m.} = 50^\circ$ were taken with a momentum bite of 5.4%. Some of the data at $\theta_{c.m.} = 110^\circ$ were taken with $\Delta p/p = 6.7\%$.

scintillation-counter telescopes located symmetrically above and below the beam line. The telescopes were sensitive to muons from pion decay in flight and to pions in the beam scattered at small angles by the vacuum windows and beam monitors.

B. Polarized proton target

A polarized proton target (PPT) was used with the axis of polarization perpendicular to the scattering plane. The target material was 1,2-propanediol ($C_3H_8O_2$). The target beads were contained in a cylindrical cell 2 cm in diameter and 4 cm long, with the pion beam incident along the axis of the cylinder. The target material was submerged in a ^3He bath at a temperature of 0.5 K. The propanediol was prepared in the form of beads about 1 mm in diameter in order to improve thermal contact with the ^3He bath and thus dissipate the heat load of the absorbed microwave radiation. The polarizing magnetic field of 2.5 T was provided by a conventional Varian magnet. The magnetic field was measured to be uniform to a few parts in 10^5 over a cylindrical central volume 4 cm high by 5 cm in diameter. This ensured a sufficiently uniform field for optimum polarization over the entire volume of the target cell. The target material contained only 0.07 g/cm^3 free protons; the ratio of free to bound protons in the target was 10.5% by mass. The free protons in the 1,2-propanediol were polarized dynamically by microwave pumping at 70 GHz. The polarization was reversed by a 0.4-GHz adjustment of the microwave frequency, keeping the magnetic field constant. The polarization of the target material was measured by an integrating nuclear-magnetic-resonance (NMR) system at a resonance frequency of approximately 106 MHz. The target polarization, typically 80%, was measured and recorded every 3–5 min during data taking. The absolute calibration of the NMR system was accomplished periodically via measurements of the thermal equilibrium polarization (P_T^0) signal at 1 K. The proton polarization in the static mag-

netic field at thermal equilibrium (microwaves off) is given by Boltzmann statistics:

$$P_T^0 = \tanh \frac{\mu_p B}{KT}, \quad (12)$$

where μ_p is the magnetic moment of the proton and B is the magnetic field strength. The uncertainty in the measurements of the thermal-equilibrium NMR signal gives rise to a $\pm 3\%$ systematic uncertainty in the target polarization. This estimate is based on our evaluation of the compound error due to (i) the thermometer calibration of the NMR shunts, (ii) a small nonlinearity in the NMR amplifier system, (iii) a thermal-molecular pressure effect, and (iv) the cleanliness of the target cell.

C. Detectors

The scattered pion and the recoil proton were detected in coincidence (except at $p_\pi = 547$ MeV/c, $\theta_{c.m.} = 120^\circ$ where only the scattered π^- was detected) using the LAMPF large-acceptance spectrometer³¹ (LAS) and a recoil detector.

The LAS is a quadrupole-quadrupole-dipole (QQD) spectrometer with a vertical bend of 30° ; thus, the scattering angle and momentum are determined in orthogonal planes. The intrinsic solid angle of the spectrometer is 25 msr. The particle trajectories in the LAS were determined using wire chambers at the entrance and exit of the quadrupole doublet and a pair of chambers following the analyzing magnet. The wire spacing is 2 mm in every plane except 4Y, in which it is 4 mm. A scintillation counter at the spectrometer entrance (S1) and two focal-plane scintillation-counter arrays (S2, S3) provided time-of-flight (TOF) and pulse-height information. Particle species were identified by TOF and pulse height in the three sets of LAS scintillators. The LAS trigger was S1·S2·S3. The overall efficiency for all eight planes of the LAS was typically 50%.

The recoil detector consisted of a wire chamber with an active area of 94 cm by 62 cm placed between two scintillator hodoscopes. The overall efficiency for the two planes of the recoil chamber was typically 90%. For each particle detected in the recoil detector the position data from the wire chamber, the pulse height in the scintillation counters, and the TOF relative to the LAS front scintillator (S1) were recorded. A coincidence between recoil front (RF) and back (RB) scintillation counters defined the recoil trigger: RF·RB. The electronics used, details of the dead-time measurement, and the operational techniques are given in Ref. 32. No data were accepted between beam pulses (beam gate off), when the run gate was off (no run in progress), or when the computer was busy. The fraction of events lost because of dead time in the computer and electronics were determined by counting the S1·S2·S3 signals in CAMAC scalers with and without a dead-time inhibit gate. The intensity of the pion beam was adjusted to keep this dead time below 20%.

The field of the polarized-target magnet causes a considerable bending of the trajectories of the incident and final-state charged particles, significantly reducing the ac-

ceptance of the LAS, particularly at the lowest momentum (471 MeV/c), where it was reduced by a factor of approximately 4. A steering magnet, Ricardo in Fig. 1, was attached to and rotated with the LAS in the PPT fringing field to increase the acceptance; this was particularly important for low-momentum scattered pions.

A related complication introduced by the polarized-target magnetic field was the offset in both the measured scattering angles and interaction vertex. As an example, for $\pi^- p \rightarrow \pi^- p$ at $\theta_{c.m.} = 62.5^\circ$ and 471 MeV/c with the magnetic field pointed down, the incident beam was deflected 18° to the right at the target. (Angles are measured relative to the undeflected incident beam direction: a positive angle indicates the beam left direction.) At $\theta_{c.m.} = 62.5^\circ$ the scattered-pion momentum is 406 MeV/c and $\theta_{lab}^\pi = -46^\circ$. The recoil-proton momentum is 347 MeV/c and $\theta_{lab}^p = 57^\circ$. The LAS first chamber was 75 cm away from the target. The 406 MeV/c scattered π^- lost 5 MeV/c in the target and bent 17° in the polarized-target magnet field to the right over this distance; therefore, the LAS was set at $\theta_{LAS} = -(18^\circ + 46^\circ + 17^\circ) = -81^\circ$ with a nominal central momentum of $406 - 5 = 401$ MeV/c. The recoil detector was located 190 cm away from the target. The recoil protons bent 34.5° in the polarized-target magnetic field to the left. Therefore, the recoil detector was set at $\theta_R = 57^\circ + 34.5^\circ - 18^\circ = 73.5^\circ$. The calculation of detector angles is based on a detailed map of the PPT magnetic field, both with and without Ricardo in place, using a NMR probe in the central region and a rotating coil in the fringe field. The estimated accuracy of these measurements is $\pm 0.5\%$.

The field direction of the polarized-target magnet was chosen at certain scattering angles so as to extend the accessible scattering-angle range: pions scattered at angles which would have missed the LAS with one setting of the magnet were deflected into the LAS for the opposite polarity.

D. Data acquisition

At each scattering angle the yield was measured with a given target spin orientation. The spin of the target was then flipped and the yield was measured for the new spin orientation. Because reversal of the polarization was accomplished by a small shift in the microwave frequency, no change in the magnitude or direction of the polarized-target magnetic field was required. Thus, "spin-up" and "spin-down" data were taken under identical kinematic conditions. For a check on systematic errors we flipped the spin according to the pattern up-down-down-up for a number of cases. The results were consistent within experimental uncertainties. For a majority of the data points only up-down was used.

The trigger for the coincidence events was S1·S2·S3·RF·RB. For each trigger we recorded the pulse height from all struck scintillators, the TOF in the LAS, the recoil-proton TOF, and the position data from all the LAS and recoil-detector wire chambers.

VI. DATA ANALYSIS

The position information from the x and y planes of the LAS wire chambers was used to calculate (i) the parti-

cle momentum, (ii) the apparent interaction point in the target (TGTX, TGT_Y), and (iii) the angle between the trajectory of the particle following the LAS bend and the central ray in both the horizontal (HANG) and vertical (VANG) planes. Parameter (ii) was used to reject events not originating in the target-cell volume and parameter (iii) was used to reject events in which the scattered pion decayed in the spectrometer. Each data run was replayed several times. Each time, cuts were applied to one more measured or calculated parameter in the following order: the LAS TOF and LAS scintillator pulse height, the recoil TOF information [time of flight to individual recoil scintillator counters with respect to S1 (TB) was measured, the timing sum (TS), and the difference (TD), between photomultiplier tubes at each end of the counters in the recoil hodoscope], the scintillator pulse height, the recoil wire-chamber data, the target projection, and the muon rejection. In the single-arm measurement (i.e., when just the pion was detected in the LAS) only the LAS TOF and pulse height, target projections, and muon rejection cuts were used. At each scattering angle, identical cuts were used for runs with the target polarization direction up and down and for the background runs. Following each pass the analyzing power was calculated from the expression

$$A_N = \frac{1}{P_T} \frac{\uparrow - \downarrow}{\uparrow + \downarrow - 2B}, \quad (13)$$

where \uparrow (\downarrow) is the polarization up (down) yield normalized to the pion decay telescope monitors and corrected for chamber efficiencies and dead time, B is the normalized background yield, and P_T is the target polarization. The value obtained for A_N in each pass was compared with its value from the previous pass for consistency. A typical set of analyzing powers following each pass is given in Table II. It illustrates that our results are independent of the cuts applied. Note that this also demonstrates that the effects of counter and wire-chamber efficiencies on analyzing powers have been properly taken into account.

The yield of good events was obtained from the pion-momentum spectrum in the LAS (after cuts had been applied). The yields were normalized to the beam monitors and corrected for chamber efficiency and dead time. The pion survival fraction over the spectrometer path length, and the solid angle, are multiplicative factors and remain

the same independent of target spin direction, and thus cancel from numerator and denominator of the asymmetry equation. The number of target nucleons per cm^2 was the same for spin-up and spin-down runs, but was slightly different for the background measurement runs; the background yield was corrected for that. The momentum spectrum of the scattered pions, as measured in the LAS, contained a prominent peak on top of a small, nearly flat background. When the normalized spin-up momentum spectrum, \uparrow , was subtracted from the normalized spin-down spectrum, \downarrow , at the same scattering angle the remaining events outside the peak region canceled out and no systematic deviation from zero was seen. This demonstrates that the systematic uncertainty in the normalization of the data runs is negligible. Taking the combination $\uparrow + \downarrow - 2B$, again only events in the peak region remained, showing that the background normalization does not contain a significant systematic error. The results of these tests are also consistent with no dependence of background yield on the target polarization, as anticipated.

A. Background

The background is mainly due to quasielastic scattering on carbon and oxygen nuclei contained in the propanediol, the ^3He and ^4He coolant, and the walls of the target cell and the cryostat. The background yield was measured in separate runs with the propanediol replaced by carbon beads with approximately the same number of carbon nuclei as in the propanediol target.

The highly overconstrained signal derived from our coincidence-detection system resulted in excellent background suppression. Even though the target material contained only 0.07 g/cm^3 hydrogen the background-to-signal ratio was typically 1/10. For the measurement in which only the pion was detected, the background-to-signal ratio was one to one.

B. Uncertainties

The data have small statistical and systematic uncertainties. The overall normalization uncertainty scales all results and arises from the uncertainty in the target-polarization calibration, which we estimate to be $\pm 3\%$ (see Sec. II B). The individual uncertainty in each deter-

TABLE II. Consistency check on the π^-p results at $625 \text{ MeV}/c$.

| 0.02–0.08 | Interval in $\cos\theta_{c.m.}$ | | | Applied cuts |
|------------------------|---------------------------------|------------------------|------------------------|---|
| | 0.08–0.14 | 0.14–0.20 | 0.20–0.26 | |
| $A_N \pm \sigma_{A_N}$ | $A_N \pm \sigma_{A_N}$ | $A_N \pm \sigma_{A_N}$ | $A_N \pm \sigma_{A_N}$ | |
| -0.62 ± 0.05 | -0.68 ± 0.03 | -0.65 ± 0.04 | -0.63 ± 0.13 | TOF, TB, TS, TD |
| -0.62 ± 0.05 | -0.67 ± 0.03 | -0.69 ± 0.04 | -0.71 ± 0.15 | Recoil X cuts added |
| -0.64 ± 0.06 | -0.68 ± 0.04 | -0.67 ± 0.04 | -0.64 ± 0.16 | Recoil Y cuts added |
| -0.64 ± 0.06 | -0.68 ± 0.03 | -0.69 ± 0.04 | -0.77 ± 0.18 | TOF, TB, TS, TD, X, Y |
| -0.63 ± 0.06 | -0.68 ± 0.03 | -0.68 ± 0.04 | -0.72 ± 0.17 | TGTX cuts added |
| -0.62 ± 0.06 | -0.67 ± 0.03 | -0.69 ± 0.04 | -0.66 ± 0.14 | TOF, TB, TS, TD, X, Y, TGTX, TGT _Y |
| -0.63 ± 0.06 | -0.67 ± 0.03 | -0.69 ± 0.04 | -0.60 ± 0.15 | HANG cuts added |

TABLE III. Analyzing powers for π^+p elastic scattering at 471 and 547 MeV/ c . Only individual uncertainties including uncertainties in counting statistics, wire-chamber efficiencies, and dead-time corrections are listed. The normalization error due to the uncertainty in the absolute target polarization is $\pm 3\%$.

| 471 MeV/ c | | | 547 MeV/ c | | |
|---------------------|-------|----------------|---------------------|-------|----------------|
| $\cos\theta_{c.m.}$ | A_N | σ_{A_N} | $\cos\theta_{c.m.}$ | A_N | σ_{A_N} |
| 0.50 | 0.18 | 0.02 | 0.52 | 0.06 | 0.03 |
| 0.42 | 0.16 | 0.02 | 0.46 | 0.10 | 0.03 |
| 0.36 | 0.16 | 0.03 | 0.37 ^a | 0.02 | 0.03 |
| 0.29 | 0.20 | 0.03 | 0.34 ^a | 0.04 | 0.03 |
| 0.15 | 0.23 | 0.03 | 0.20 | 0.05 | 0.03 |
| 0.07 | 0.27 | 0.04 | 0.13 | 0.04 | 0.05 |
| -0.05 | 0.32 | 0.05 | 0.03 ^a | 0.09 | 0.04 |
| -0.12 | 0.22 | 0.05 | -0.02 ^a | 0.14 | 0.04 |
| -0.31 | 0.19 | 0.06 | -0.32 | -0.11 | 0.05 |
| -0.52 | -0.18 | 0.04 | -0.47 | -0.30 | 0.06 |
| -0.70 | -0.18 | 0.04 | -0.53 | -0.40 | 0.06 |
| -0.90 | -0.06 | 0.04 | -0.72 | -0.27 | 0.03 |

^aProtons were detected in the LAS.

mination of A_N is given by

$$\sigma_{A_N} = \frac{2}{P_T(\uparrow + \downarrow - 2B)^2} [(\downarrow - B)^2\sigma_{\uparrow}^2 + (\uparrow - B)^2\sigma_{\downarrow}^2 + (\uparrow - \downarrow)^2\sigma_B^2]^{1/2}, \quad (14)$$

where \uparrow , \downarrow , and B are normalized yields as defined in Eq. (13) and σ_{\uparrow} is the uncertainty in \uparrow , etc. This uncertainty includes the statistical counting uncertainty and the uncertainties in the chamber efficiencies and dead time.

VII. RESULTS

The analyzing power A_N for π^+p and π^-p elastic scattering measured in this experiment are listed in Tables III–VI and presented graphically in Figs. 2 and 3. Only the individual uncertainties in A_N , as discussed in the preceding paragraph, are presented. The large horizontal angular acceptance (9°) of the LAS combined with its siz-

able momentum acceptance allows us to divide the momentum spectrum into two or three bins. The centroid of each bin was determined separately. The average pion scattering angle was calculated from the momentum centroid taking into account the energy loss in the target and in the LAS; each momentum bin was converted into an angular interval. This indirect determination of the pion scattering angle avoids the complications introduced by the finite target length and the strong bending of the pions in the field of the polarized-target magnet.

The general features of the angular distributions of π^+p analyzing powers do not vary greatly from 471 to 625 MeV/ c , except that at $\cos\theta_{c.m.} = -0.4$, where A_N increases gradually from -0.2 to -0.8 . There is a dramatic change, however, in A_N between 625 and 687 MeV/ c , illustrating the great sensitivity of the analyzing power to the energy dependence of the partial waves. It is imperative for an accurate determination of A_N that the beam-momentum calibration is well established and that the

TABLE IV. Analyzing powers for π^+p elastic scattering at 625 and 687 MeV/ c (see caption for Table III).

| 625 MeV/ c | | | 687 MeV/ c | | |
|---------------------|-------|----------------|---------------------|-------|----------------|
| $\cos\theta_{c.m.}$ | A_N | σ_{A_N} | $\cos\theta_{c.m.}$ | A_N | σ_{A_N} |
| 0.67 | 0.00 | 0.04 | 0.54 ^a | -0.10 | 0.06 |
| 0.61 | -0.01 | 0.07 | 0.49 ^a | -0.11 | 0.06 |
| 0.42 ^a | -0.03 | 0.04 | 0.25 ^a | -0.12 | 0.07 |
| 0.40 ^a | -0.09 | 0.04 | 0.21 ^a | -0.17 | 0.08 |
| 0.22 | -0.04 | 0.05 | 0.18 ^a | -0.24 | 0.10 |
| 0.16 | -0.10 | 0.05 | -0.13 | -0.19 | 0.05 |
| -0.23 | -0.48 | 0.12 | -0.19 | -0.09 | 0.06 |
| -0.30 | -0.55 | 0.14 | -0.38 | 0.13 | 0.15 |
| -0.51 | -0.74 | 0.16 | -0.69 | -0.14 | 0.10 |
| -0.56 | -0.70 | 0.15 | -0.73 | -0.17 | 0.11 |
| -0.87 | -0.29 | 0.16 | -0.92 | -0.29 | 0.06 |

^aProtons were detected in the LAS.

TABLE V. Analyzing powers for π^-p elastic scattering at 471 and 547 MeV/c (see caption for Table III).

| 471 MeV/c | | | 547 MeV/c | | |
|---------------------|-------|----------------|---------------------|-------|----------------|
| $\cos\theta_{c.m.}$ | A_N | σ_{A_N} | $\cos\theta_{c.m.}$ | A_N | σ_{A_N} |
| 0.50 | -0.82 | 0.02 | 0.59 | -0.75 | 0.04 |
| 0.44 | -0.81 | 0.02 | 0.55 | -0.73 | 0.03 |
| 0.35 | -0.80 | 0.02 | 0.46 | -0.85 | 0.02 |
| 0.28 | -0.72 | 0.02 | 0.31 | -0.78 | 0.03 |
| 0.14 | -0.57 | 0.02 | 0.24 | -0.80 | 0.03 |
| 0.07 | -0.47 | 0.02 | 0.13 | -0.64 | 0.03 |
| -0.02 | -0.33 | 0.03 | 0.08 | -0.61 | 0.02 |
| -0.08 | -0.19 | 0.03 | 0.03 | -0.55 | 0.03 |
| -0.49 | 0.66 | 0.07 | -0.06 | -0.40 | 0.06 |
| -0.55 | 0.67 | 0.09 | -0.11 | -0.40 | 0.09 |
| -0.70 | 0.59 | 0.06 | -0.26 | 0.27 | 0.10 |
| -0.90 | 0.49 | 0.04 | -0.47 ^a | 0.75 | 0.09 |
| | | | -0.53 ^a | 0.96 | 0.09 |
| | | | -0.73 | 0.57 | 0.04 |
| | | | -0.77 | 0.44 | 0.05 |
| | | | -0.89 | 0.18 | 0.03 |

^aSingle-arm measurement (only the pion was detected in the LAS).

spread in beam momentum is small and well known.

The general features of the π^-p analyzing-power angular distribution are rather similar at 471, 547, and 625 MeV/c. As the incident beam momentum increases the large positive peak seen at backward angles in $A_N(\pi^-p \rightarrow \pi^-p)$ shifts forward and is compressed in width. The most striking change occurs between 625 and 687 MeV/c, leading to a second minimum at backward angles at 687 MeV/c.

A. Comparison with partial-wave analyses

In Figs. 2 and 3 our A_N data are compared to the results of the three PWA's (Refs. 24–26). At 471 MeV/c the agreement between each PWA result and our $A_N(\pi^-p \rightarrow \pi^-p)$ data is good. At 547 and 625 MeV/c the PWA's generally reproduce the overall angular distribution of the data; the agreement is a little better at forward angles for the VPI analysis than the other two anal-

yses. Finally, at 687 MeV/c, the KH and VPI groups predict a large maximum near $\cos\theta_{c.m.} = -0.4$. The data show a maximum that is not as high as KH or VPI. The disagreement is only of the order of 1.5 standard deviations (SD) with the VPI PWA, but the data do not support the KH PWA at 687 MeV/c at backward angles.

All three PWA predictions for $A_N(\pi^-p \rightarrow \pi^-p)$ at 471, 547, and 625 MeV/c approach -1.0 at forward angles, but our data show somewhat smaller magnitudes. The agreement with the data at 471 MeV/c is good beyond 60° , with the exception of the most backward angle, where the disagreement is 5 SD. At 547 MeV/c the agreement is good at large angles but differences of as much as 6 SD are seen at forward angles. At 625 MeV/c the disagreement at large angles is of the order of 5 SD and at forward angles up to 9 SD. Finally, at 687 MeV/c the agreement is good at forward angles, with differences of 4 SD at backward angles. For a numerical comparison we have calculated

TABLE VI. Analyzing powers for π^-p elastic scattering at 625 and 687 MeV/c (see caption for Table III).

| 625 MeV/c | | | 687 MeV/c | | |
|---------------------|-------|----------------|---------------------|-------|----------------|
| $\cos\theta_{c.m.}$ | A_N | σ_{A_N} | $\cos\theta_{c.m.}$ | A_N | σ_{A_N} |
| 0.62 | -0.81 | 0.03 | 0.67 | -0.50 | 0.06 |
| 0.54 | -0.91 | 0.04 | 0.63 | -0.53 | 0.03 |
| 0.41 | -0.80 | 0.01 | 0.59 | -0.57 | 0.05 |
| 0.33 | -0.78 | 0.02 | 0.44 ^a | -0.68 | 0.05 |
| 0.18 | -0.70 | 0.04 | 0.39 ^a | -0.72 | 0.04 |
| 0.11 | -0.66 | 0.03 | 0.18 ^a | -0.81 | 0.09 |
| -0.30 | 0.34 | 0.06 | 0.14 ^a | -0.79 | 0.08 |
| -0.36 | 0.52 | 0.08 | -0.31 | 0.31 | 0.08 |
| -0.75 | 0.13 | 0.05 | -0.36 | 0.05 | 0.05 |
| -0.79 | 0.14 | 0.04 | -0.77 | -0.30 | 0.05 |
| | | | -0.80 | -0.27 | 0.06 |
| | | | -0.94 | -0.17 | 0.04 |

^aProtons were detected in the LAS.

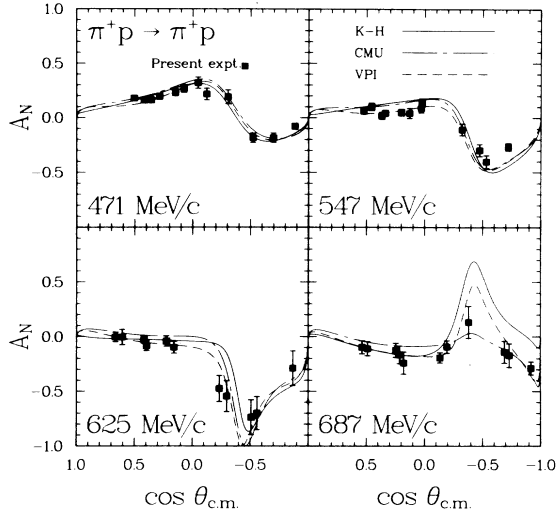


FIG. 2. Analyzing power A_N measured in π^+p elastic scattering using a transversely polarized target. The incident pion momenta are 471, 547, 625, and 687 MeV/c. The curves are the results of the partial-wave analyses of Refs. 24 (solid curve), 25 (chain-dashed curve), and 26 (dashed curve).

$$\chi^2 = \frac{1}{N} \sum \frac{(A_N - A_N^{\text{PWA}})^2}{\sigma_{A_N}^2},$$

where A_N^{PWA} is the analyzing power obtained from the partial-wave analyses. The results are given in Table VII. The consistency of the PWA's with our data is much worse for π^-p than for π^+p elastic scattering. Generally speaking, the previously existing π^-p data, on which these PWA's are based, are sparser and of lower quality than the π^+p data; poorer agreement with our π^-p data may merely reflect this fact.

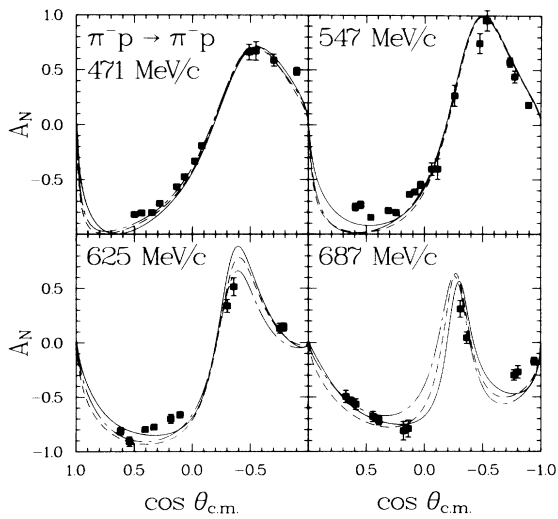


FIG. 3. Analyzing power A_N measured in π^-p elastic scattering (see caption for Fig. 2).

TABLE VII. A numerical comparison of χ^2 (see text) of our data with various PWA predictions using only individual uncertainties in the data.

| Momentum (MeV/c) | | KH | CMU-LBL | VPI (FP84) |
|------------------|---------|------|---------|------------|
| 471 | π^+ | 1.2 | 2.2 | 1.4 |
| 471 | π^- | 14.6 | 4.8 | 8.9 |
| 547 | π^+ | 6.8 | 4.3 | 2.6 |
| 547 | π^- | 10.5 | 14.9 | 19.0 |
| 625 | π^+ | 2.1 | 2.2 | 0.6 |
| 625 | π^- | 10.5 | 17.9 | 25.2 |
| 687 | π^+ | 4.9 | 1.3 | 0.7 |
| 687 | π^- | 6.7 | 6.7 | 7.1 |

B. Transversity cross sections

Transversity cross sections are an alternative to the analyzing powers as a presentation of our results. The transversity cross sections are just the differential cross sections from a target with 100% transverse polarization. Parallel and antiparallel transversity cross sections are given by Eqs. (2) and (3), respectively, with $P_T=1$. We have

$$I_+ = I_0(1 + A_N), \quad (15)$$

$$I_- = I_0(1 - A_N), \quad (16)$$

where I_0 is the unpolarized differential cross section. Transversity cross sections provide a more sensitive test of isospin invariance than do unpolarized cross sections. We combine our separate measurements of the differential cross section⁵ I_0 and our present results for the analyzing power A_N at the same beam momenta to obtain the transversity cross sections. However, I_0 and A_N have been measured at different scattering angles. To obtain the transversity cross sections as a function of c.m. scattering angle we have used the following procedure.

(a) The differential cross sections were fitted to Legendre polynomials in $\theta_{c.m.}$.

(b) This fit was used to interpolate to angles where we have measured A_N , and I_+ and I_- were obtained with appropriate uncertainties.

(c) Legendre-polynomial fits to I_+ and I_- were calculated.

Because $A_N=0$ at 0° and 180° , constraints were added to the fitting procedure which forced $I_+=I_-=I_0$ at these angles. Another constraint was added at angles where I_0 was measured which did not allow the fit for $I_\pm(\theta)$ to assume values that would require $|A_N| \geq 1$. I_+ and I_- were fitted simultaneously in the least-squares sense. The Legendre coefficients for $I_+(\theta)$ and $I_-(\theta)$ are given in Tables VIII and IX, respectively,

$$I_+(\theta) = c_0 + c_1 P_1(\cos\theta) + c_2 P_2(\cos\theta) + \dots,$$

$$I_-(\theta) = c'_0 + c'_1 P_1(\cos\theta) + c'_2 P_2(\cos\theta) + \dots.$$

The measured values and fits for I_+ , I_- , and I_0 are graphed in Figs. 4 and 5. Note that for π^+p the parallel transversity cross sections at 547 and 625 MeV/c show a

TABLE VIII. Coefficients of Legendre-polynomial fit to parallel transversity cross section (mb/sr).

| Momentum (MeV/c) | | c_0 | c_1 | c_2 | c_3 | c_4 | c_5 |
|---------------------|---------|-----------------|------------------|-----------------|------------------|------------------|------------------|
| 471 | π^+ | 3.41 ± 0.14 | 4.36 ± 0.34 | 3.57 ± 0.42 | -0.29 ± 0.32 | -0.05 ± 0.20 | |
| 471 | π^- | 0.55 ± 0.04 | -0.27 ± 0.09 | 0.46 ± 0.11 | 0.27 ± 0.09 | 0.07 ± 0.06 | |
| 547 | π^+ | 2.02 ± 0.10 | 3.24 ± 0.21 | 2.33 ± 0.30 | 0.02 ± 0.19 | -0.10 ± 0.14 | |
| 547 | π^- | 0.56 ± 0.01 | -1.08 ± 0.05 | 0.19 ± 0.10 | 1.22 ± 0.20 | 0.62 ± 0.26 | |
| 625 | π^+ | 1.20 ± 0.03 | 2.10 ± 0.08 | 1.60 ± 0.43 | 0.69 ± 0.67 | -0.26 ± 1.02 | -0.25 ± 1.26 |
| 625 | π^- | 0.58 ± 0.06 | 0.12 ± 0.22 | 1.07 ± 0.20 | 0.28 ± 0.33 | 0.47 ± 0.12 | 0.50 ± 0.18 |
| 687 | π^+ | 0.97 ± 0.15 | 1.82 ± 0.39 | 1.25 ± 0.49 | 0.26 ± 0.42 | -0.13 ± 0.25 | 0.02 ± 0.09 |
| 687 | π^- | 0.90 ± 0.08 | 1.13 ± 0.20 | 2.12 ± 0.27 | 0.74 ± 0.28 | 0.77 ± 0.21 | 0.15 ± 0.12 |

much more pronounced minimum than the antiparallel transversity cross section, but otherwise have the same features. For π^-p the parallel and antiparallel transversity cross-section angular distributions are quite different.

C. Triangle-inequality bounds

The Legendre polynomial fits for I_+ and I_- discussed in the preceding subsection were used to obtain the upper and lower bounds of the triangle inequality equations (10) and (11). This procedure gives a natural way of obtaining the uncertainties in the bounds. The values obtained from the measurements of A_N and the fits to the upper and lower bounds for parallel and antiparallel transversity cross sections are shown in Figs. 6 and 7. When transversity cross sections for CEX at our beam energies become available, they can be used directly for a model-independent test of isospin invariance.

D. Comparison with previous experiments

There are two data sets^{33,34} in the literature for A_N in π^+p elastic scattering at momenta near the upper end of the range of the present measurements. The experiment by Martin *et al.*³³ covers many incident pion momenta, including 603, 617, 660, 674, and 708 MeV/c, and many scattering angles; however, the uncertainties at backward angles are usually ± 0.3 and often larger; this limits the usefulness of these data. A comparison of the Martin results at 617 MeV/c with our data at 625 MeV/c is shown in Fig. 8(a). The Martin data agree with our work within the large errors of the former, except near

$\cos\theta_{c.m.} = -0.3$. In view of the rapid variation of A_N a comparison at other momenta is not very meaningful. Also shown in Fig. 8(a) are the recoil-proton polarization data at 492 MeV (616 MeV/c) by Bareyre *et al.*³⁵ These data for the recoil-proton polarization (P), which is equivalent to our analyzing power data by the $P=A$ theorem. The agreement is reasonable, keeping in mind the strong momentum dependence of A_N and the uncertainties in Bareyre's results associated with the use of limited analyzing-power data for carbon in their experiment. The measurements by Abaev *et al.*³⁴ at 455–705 MeV/c are restricted to scattering angles larger than 100° with typical uncertainties of ± 0.1 . In Fig. 8(b) we compare the Abaev data at 685 MeV/c to ours at 687 MeV/c; the agreement is good. In Fig. 8(c) our 625-MeV/c π^- data are compared with the work of Bareyre *et al.*,³⁶ at 616 MeV/c. Again, agreement with our data is reasonable. Comparison of our π^-p data at 687 MeV/c with the data of Bekrenev *et al.*³⁷ at 685 MeV/c shows good agreement at forward angles, but the Bekrenev results are slightly larger than our measurements at backward angles [see Fig. 8(d)]. Given the trend of the angular distributions with incident beam momentum, the differences could be accounted for by an upward shift of a few MeV/c in the central beam momentum of the results of Bekrenev *et al.* The results of Martin *et al.*,³³ Abaev *et al.*,³⁴ Bareyre *et al.*,^{35,36} and Bekrenev *et al.*³⁷ are not in conflict with our more precise data.

Other measurements of A_N at energies in the region of our data have been reported in the literature by Cox *et al.*,³⁸ Bizard *et al.*,³⁹ Chamberlain *et al.*,⁴⁰ and Arens *et al.*,⁴¹ a measurement of the polarization parameter in

TABLE IX. Coefficients of Legendre-polynomial fit to antiparallel transversity cross section (mb/sr).

| Momentum (MeV/c) | | c'_0 | c'_1 | c'_2 | c'_3 | c'_4 | c'_5 |
|---------------------|---------|-----------------|-----------------|-----------------|------------------|------------------|------------------|
| 471 | π^+ | 2.96 ± 0.14 | 3.56 ± 0.34 | 4.08 ± 0.42 | 0.51 ± 0.32 | -0.12 ± 0.20 | |
| 471 | π^- | 0.94 ± 0.04 | 0.94 ± 0.09 | 0.29 ± 0.11 | -0.94 ± 0.09 | -0.14 ± 0.06 | |
| 547 | π^+ | 1.99 ± 0.10 | 3.06 ± 0.21 | 2.50 ± 0.30 | 0.21 ± 0.19 | -0.25 ± 0.14 | |
| 547 | π^- | 1.04 ± 0.01 | 2.12 ± 0.05 | 1.01 ± 0.10 | -1.99 ± 0.20 | -0.68 ± 0.26 | |
| 625 | π^+ | 1.35 ± 0.03 | 2.24 ± 0.08 | 1.35 ± 0.43 | -0.59 ± 0.67 | -0.16 ± 1.02 | 0.52 ± 1.26 |
| 625 | π^- | 1.39 ± 0.06 | 1.68 ± 0.22 | 1.20 ± 0.20 | -0.93 ± 0.33 | -0.48 ± 0.12 | -0.14 ± 0.18 |
| 687 | π^+ | 1.12 ± 0.15 | 2.00 ± 0.39 | 1.22 ± 0.49 | 0.02 ± 0.42 | -0.25 ± 0.25 | 0.07 ± 0.09 |
| 687 | π^- | 1.92 ± 0.08 | 2.31 ± 0.20 | 2.38 ± 0.27 | 0.74 ± 0.28 | -0.50 ± 0.21 | 0.04 ± 0.12 |

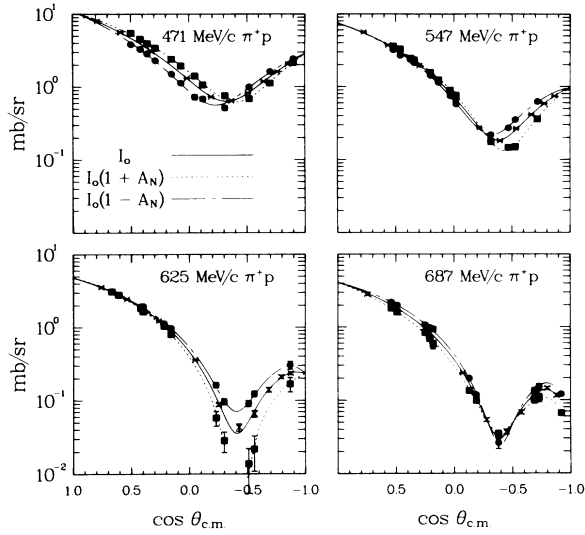


FIG. 4. Unpolarized, parallel, and antiparallel transversity cross sections for π^+p elastic scattering. In each case the symbols represent measured values and the curve represents a Legendre-polynomial fit to the measurements. The crosses and solid curve represent the unpolarized cross sections; the solid squares and dashed curve represent the parallel transversity cross sections; the solid circles and chain-dashed curve represent the antiparallel cross sections.

this region has been made by Eandi *et al.*⁴² and Dickinson *et al.*⁴³ The results of these experiments contain systematic errors of $\pm 10\%$ and therefore have minimal influence on the PWA's compared to this experiment. These data are consistent in shape with our measurements.

The improved precision of our measurements compared to earlier experiments is attributed to improvement in two primary areas.

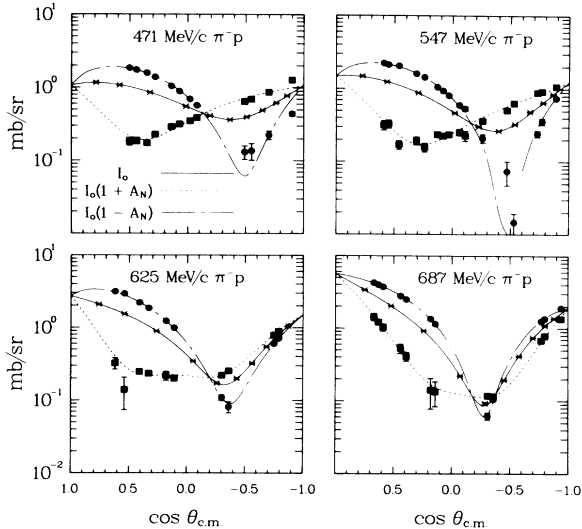


FIG. 5. Unpolarized, parallel, and antiparallel transversity cross sections for π^-p elastic scattering (see caption for Fig. 4).

(1) *Signal-to-background ratio.* For coincidence events in the present experiment the measured parameters were the momentum, polar angle, and azimuthal angle of the particle detected in the LAS, and the polar and azimuthal angles of the particle detected in the recoil arm. Because the LAS bend plane is vertical, the particle momentum and the scattering angle are determined independently. For the particles detected in the LAS, momentum and TOF measurements allow unambiguous particle identification; in addition, the pulse height in the scintillation counters was measured. Identification of the particles detected in the recoil arm was accomplished using TOF with respect to the LAS front scintillator and pulse height in the scintillator counters. These measurements result in a highly overconstrained signal, compared to earlier measurements.

(2) *Polarized target.* In some of the earlier experiments, the target material, LMNO_3 , provided only about 50% polarization, with a very low free-hydrogen-to-bound-nucleon ratio. Measurements of background and normalization of background to polarized-target yields were notoriously difficult. By contrast, the target used in the present experiment typically allowed polarization of 80%, and the background measurements could be carried out using graphite beads whose density is matched to the density of carbon in propanediol. Improvements in NMR techniques allowed the polarization to be determined with an overall uncertainty of only 3%.

VIII. INFLUENCE ON VPI PHASE SHIFTS

Using the VPI scattering analysis interactive dial-in (SAID) program we added our data to the existing database for single-energy PWA's. Shown in Tables X and XI are listings of the πN scattering phase shifts in the existing VPI PWA and the new phases as a result of the addition of our data to their database. At 471 MeV/c (352 MeV) the single-energy solution C35, valid at 330–370

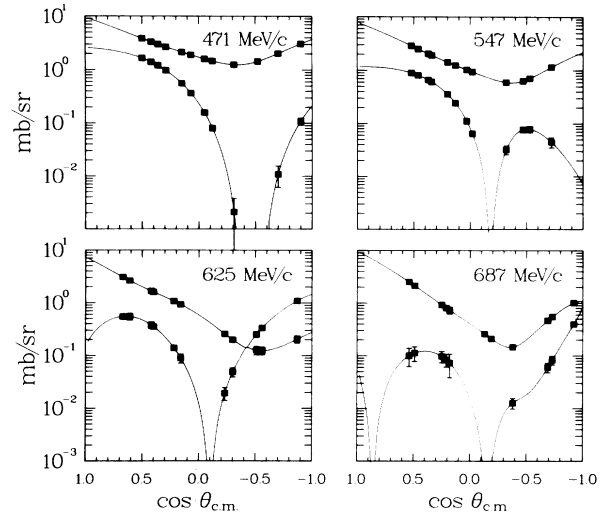


FIG. 6. Upper and lower bounds of the triangle inequality for parallel transversity cross sections. See Eq. (10).

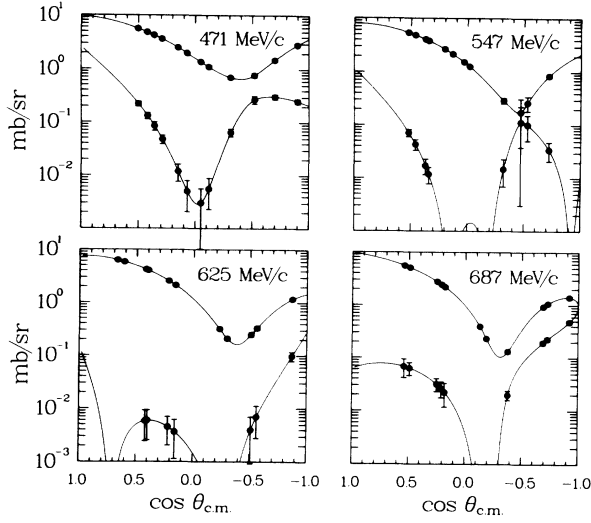


FIG. 7. Upper and lower bounds of the triangle inequality for antiparallel transversity cross sections. See Eq. (11).

MeV, was used. The single-energy solution C40 applies to 375–425 MeV, while C45 is used for 425–475 MeV. The 547 MeV/c (425 MeV) is right at the boundary of the C40 and C45 solutions. We have added our 547-MeV/c data to both C40 and C45. The effect of our data at 625 MeV/c (501 MeV) and 687 MeV/c (561 MeV) on C50 and C55, respectively, is also given. The results for $\pi^-p \rightarrow \pi^-p$ are summarized in Table XI.

The effect of our $A_N(\pi^+p \rightarrow \pi^+p)$ data on various phases is small, indicating that the isospin $I = \frac{3}{2}$ πN amplitudes in our energy region are reasonably well understood. Whereas in $\pi^+p \rightarrow \pi^+p$ scattering only $I = \frac{3}{2}$ amplitudes are involved, in $\pi^-p \rightarrow \pi^-p$ both $I = \frac{1}{2}$ and $\frac{3}{2}$ amplitudes contribute; see Eqs. (7). Thus, the addition of our $A_N(\pi^-p \rightarrow \pi^-p)$ data to the VPI database for single-energy solutions is expected to affect only the $I = \frac{1}{2}$ phase shifts; this is indeed observed. The effects are the largest at 687 MeV/c, where the P_{11} phase increases from 86° to 98°.

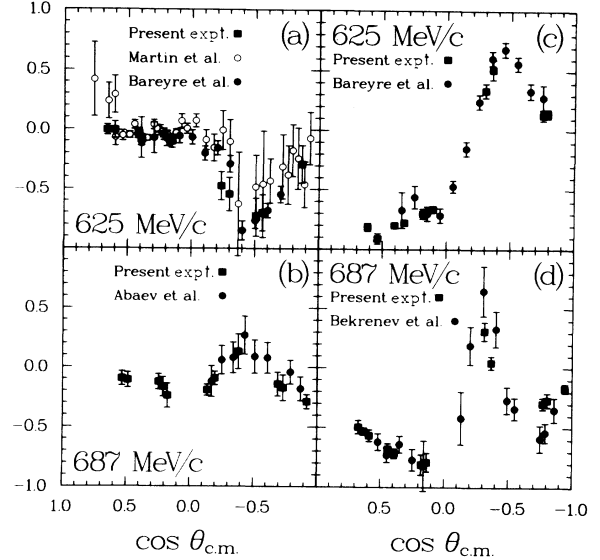


FIG. 8. (a) Results of the present experiment at 625 MeV/c π^+ compared to the data of Martin *et al.* (Ref. 33) at 617 MeV/c and Bareyre *et al.* (Ref. 35) at 616 MeV/c. (b) Results of the present experiment at 687 MeV/c π^+ compared with the data of Abaev *et al.* (Ref. 34) at 685.5 MeV/c. (c) Comparison of present data at 625 MeV/c π^- with those of Bareyre *et al.* (Ref. 36) at 616 MeV/c (492 MeV). (d) Comparison of present data at 687 MeV/c π^- with those of Bekrenev *et al.* (Ref. 37) at 685.5 MeV/c (560 MeV).

IX. SUMMARY AND CONCLUSION

We have measured the analyzing power A_N in π^+p and π^-p elastic scattering at 471, 547, 625, and 687 MeV/c. The data have been transformed to transversity cross sections using separate measurements of the unpolarized differential cross section; these were used to obtain the bounds of the triangle inequalities for a convenient test of isospin invariance. Our A_N data are compared with the predictions of the three most recent PWA's and with the results of previous experiments.

TABLE X. Effect of the addition of our π^+p data on the VPI single-energy solutions. Phases are in degrees.

| Phase | 471 MeV/c (C35) | | 547 MeV/c (C40) | | 547 MeV/c (C45) | | 625 MeV/c (C50) | | 687 MeV/c (C55) | |
|----------|--------------------|-------|--------------------|-------|--------------------|-------|--------------------|-------|--------------------|-------|
| | Old | New |
| S_{11} | 13.1 | 13.1 | 14.6 | 14.6 | 16.3 | 16.2 | 17.5 | 17.4 | 28.5 | 28.5 |
| S_{31} | -23.9 | -23.9 | -25.7 | -25.6 | -26.9 | -26.8 | -27.8 | -27.8 | -28.7 | -28.6 |
| P_{11} | 26.7 | 26.7 | 39.2 | 39.1 | 47.9 | 48.2 | 56.0 | 55.9 | 86.0 | 86.0 |
| P_{13} | -4.6 | -4.6 | -4.3 | -4.3 | -6.3 | -6.2 | -7.7 | -7.7 | -6.4 | -6.4 |
| P_{31} | -10.0 | -10.0 | -12.0 | -11.9 | -13.0 | -12.9 | -14.4 | -14.4 | -15.7 | -15.6 |
| P_{33} | 142.2 | 142.2 | 148.3 | 148.3 | 152.8 | 152.8 | 157.4 | 157.3 | 161.2 | 161.0 |
| D_{13} | 6.8 | 6.8 | 9.8 | 9.8 | 15.1 | 15.2 | 23.7 | 23.8 | 36.5 | 36.5 |
| D_{15} | | | | | 4.2 | 4.2 | 5.3 | 5.3 | 6.9 | 6.9 |
| D_{33} | | | | | 10.1 | 8.2 | 0.3 | 0.3 | 1.1 | 1.0 |
| F_{15} | | | | | | | 5.2 | 5.2 | 6.5 | 6.5 |

TABLE XI. Effect of the addition of our π^-p data on the VPI single-energy solutions. Phases are in degrees.

| Phase | 471 MeV/c (C35) | | 547 MeV/c (C40) | | 547 MeV/c (C45) | | 625 MeV/c (C50) | | 687 MeV/c (C55) | |
|----------|--------------------|-------|--------------------|-------|--------------------|-------|--------------------|-------|--------------------|-------|
| | Old | New |
| S_{11} | 13.1 | 12.8 | 14.6 | 14.8 | 16.3 | 16.4 | 17.5 | 17.2 | 26.5 | 28.0 |
| S_{31} | -23.9 | -26.9 | -25.7 | -25.7 | -26.9 | -26.9 | -27.8 | -27.8 | -28.7 | -26.6 |
| P_{11} | 26.7 | 26.9 | 39.2 | 38.9 | 47.9 | 48.1 | 56.0 | 54.0 | 86.0 | 98.1 |
| P_{13} | -4.6 | -4.7 | -4.3 | -4.5 | -6.3 | -6.2 | -7.7 | 8.0 | -6.4 | -4.8 |
| P_{31} | -10.0 | -10.0 | -12.0 | -12.0 | -13.0 | -13.0 | -14.3 | -14.3 | -15.7 | -15.7 |
| P_{33} | 142.2 | 142.2 | 148.3 | 148.4 | 152.8 | 152.9 | 157.4 | 157.4 | 161.2 | 161.2 |
| D_{13} | 6.8 | 6.7 | 9.8 | 9.9 | 15.1 | 15.1 | 23.7 | 24.1 | 36.5 | 37.1 |
| D_{15} | | | | | 4.2 | 4.3 | 5.3 | 4.7 | 6.9 | 6.2 |
| D_{33} | | | | | 0.2 | 0.2 | 0.3 | 0.3 | 1.1 | 1.1 |
| F_{15} | | | | | | | 5.2 | 5.1 | 6.5 | 6.2 |

The results of all three PWA's for π^+ data are in acceptable agreement with our analyzing-power data up to 625 MeV/c, suggesting that our measurements, together with our cross-section measurements at these and other beam momenta, present no evidence for new Δ resonances with mass less than 1450 MeV. A new PWA that incorporates our data is needed before a definite conclusion can be drawn concerning the possibility of higher-mass resonances up to 1490 MeV.

ACKNOWLEDGMENTS

We gratefully acknowledge the loan of the polarized-proton target by J. E. Simmons and the LANL P-Division and the extensive help of J. G. J. Boissevain, J. Holt, and

W. B. Tippens in the initial setup of the target. We appreciate the efforts of R. Damjanovich and the MP-8 crew and A. Kirby in mounting the experiment. We value the support rendered by J. F. Davis in the planning stages of the experiment and R. Ziocok's help with the data analysis. Finally, we thank R. Koch, who supplied the code used to generate values of A_N from the KH phase shifts, and R. A. Arndt who provided a similar code (SAID) for the VPI and CMU-LBL phase shifts. This work was supported in part by the U.S. Department of Energy. W. J. Briscoe acknowledges the partial support of the National Science Foundation and the George Washington University Committee on Research during the latter stages of the experiment. M. E. Sadler wishes to acknowledge support from the Research Council of Abilene Christian University.

*Present address: Department of Physics, George Washington University, Washington, D.C. 20052.

†Deceased.

‡Present address.

¹Particle Data Group, Phys. Lett. **170B**, 1 (1986).

²G. Höhler, *Pion-Nucleon Scattering*, edited by H. Schopper (Landolt-Börnstein, Vol. I/9b2) (Springer, Berlin, 1983).

³A. Mokhtari, W. J. Briscoe, A. D. Eichon, D. H. Fitzgerald, G. J. Kim, B. M. K. Nefkens, J. A. Wightman, S. D. Adrian, M. E. Sadler, and T. Walker, Phys. Rev. Lett. **55**, 359 (1985).

⁴A. Mokhtari, W. J. Briscoe, A. D. Eichon, D. H. Fitzgerald, G. J. Kim, B. M. K. Nefkens, J. A. Wightman, and M. E. Sadler, Phys. Rev. D **33**, 296 (1986).

⁵M. E. Sadler, C. J. Seftor, F. O. Borchering, W. J. Briscoe, D. H. Fitzgerald, P. F. Glodis, R. P. Haddock, and B. M. K. Nefkens, Phys. Lett. **119B**, 69 (1982); and (unpublished).

⁶A. Chodos, R. L. Jaffe, K. Johnson, C. B. Thorn, and V. F. Weisskopf, Phys. Rev. D **9**, 3471 (1974).

⁷T. DeGrand and C. Rebbi, Phys. Rev. D **17**, 2358 (1978).

⁸E. Umland, I. Duck, and W. von Witsch, Phys. Rev. D **27**, 2678 (1983).

⁹K. C. Bowler and A. J. G. Hey, Phys. Lett. **69B**, 469 (1977).

¹⁰F. E. Close and R. R. Horgan, Nucl. Phys. **B164**, 413 (1980).

¹¹A. De Rújula, H. Georgi, and S. L. Glashow, Phys. Rev. D

12, 147 (1975).

¹²R. Koniuk and N. Isgur, Phys. Rev. D **21**, 1868 (1980).

¹³T. Barnes and F. E. Close, Phys. Lett. **116B**, 365 (1982); **123B**, 89 (1983).

¹⁴M. Chanowitz and S. Sharpe, Nucl. Phys. **B222**, 211 (1983).

¹⁵E. Golowich, E. Haqq, and G. Karl, Phys. Rev. D **28**, 160 (1983).

¹⁶W. N. Cottingham, M. Lacombe, B. Loiseau, J. M. Richard, and R. Vinh Mau, Phys. Rev. D **8**, 800 (1973).

¹⁷F. Hussain and M. S. Sri Ram, Phys. Rev. Lett. **55**, 1169 (1985).

¹⁸M. P. Mattis and M. Karliner, Phys. Rev. D **31**, 2833 (1985); M. P. Mattis and M. E. Peskin, *ibid.* **32**, 58 (1985); M. Karliner and M. P. Mattis, Phys. Rev. Lett. **56**, 428 (1986).

¹⁹A. Hayashi, G. Eckart, G. Holzwarth, and H. Walliser, Phys. Lett. **147B**, 5 (1984).

²⁰K. F. Liu, J. S. Zhang, and G. R. E. Black, Phys. Rev. D **30**, 2015 (1984).

²¹J. D. Breit and C. R. Nappi, Phys. Rev. Lett. **53**, 889 (1984).

²²I. Zahed, U.-G. Meissner, and U. B. Kaulfuss, Nucl. Phys. **A426**, 525 (1984).

²³B. Blankleider and G. E. Walker, Phys. Lett. **152B**, 291 (1985).

²⁴G. Höhler, F. Kaiser, R. Koch, and E. Pietarinen, *Handbook*

- of Pion-Nucleon Scattering* (Physics Data No. 12-1) (Fachsinformationszentrum, Karlsruhe, 1979); R. Koch and E. Pietarinen, Nucl. Phys. **A336**, 331 (1980).
- ²⁵R. E. Cutkosky, R. E. Hendrick, J. W. Alcock, Y. A. Chao, R. G. Lipes, J. C. Sandusky, and R. L. Kelly, Phys. Rev. D **20**, 2804 (1979); R. E. Cutkosky, C. P. Forsyth, R. E. Hendrick, and R. L. Kelly, *ibid.* **20**, 2839 (1979).
- ²⁶R. A. Arndt, J. M. Ford, and L. D. Roper, Phys. Rev. D **32**, 1085 (1985).
- ²⁷R. Ayed, Saclay Report No. CEA-N-1921, 1976 (unpublished).
- ²⁸R. D. Werbeck and R. J. Macek, IEEE Trans. Nucl. Sci. **NS-22**, 1598 (1975); J. Hudomalj, D. Mann, N. D. Gabitzsch, C. Bordner, and R. Macek, Nucl. Instrum. Methods **126**, 1 (1975); N. D. Gabitzsch, D. Mann, G. Pfeufer, G. C. Phillips, J. Hudomalj, L. Y. Lee, M. Warneke, J. C. Allred, R. J. Macek, and R. Werbeck, *ibid.* **126**, 7 (1975).
- ²⁹D. Roeder and R. J. Macek, Los Alamos National Laboratory Report No. LA-7268-PR, 1977 (unpublished), pp. 31 and 32.
- ³⁰W. J. Briscoe, D. H. Fitzgerald, B. M. K. Nefkens, and M. E. Sadler, Nucl. Instrum. Methods **197**, 277 (1982).
- ³¹E. Colton, Nucl. Instrum. Methods **178**, 95 (1980).
- ³²A. Mokhtari, Ph.D. thesis, University of California, Los Angeles, 1984; Los Alamos Report No. LA-10451-T.
- ³³J. F. Martin, J. C. Sleeman, R. M. Brown, P. J. Duke, W. M. Evans, E. S. Groves, R. E. Hill, W. R. Holley, D. P. Jones, J. Thresher, and M. W. Tyrrell, Nucl. Phys. **B89**, 253 (1975).
- ³⁴V. V. Abaev, V. S. Bekrenev, Yu. A. Beloglazov, V. G. Gaditsky, A. I. Kovalev, S. P. Kruglov, A. A. Kulbardis, I. V. Lopatin, A. N. Prokofiev, V. V. Sumachev, V. Yu. Trautman, E. P. Fedorova-Koval, E. A. Filimonov, and A. V. Shvedchikov, Z. Phys. A **311**, 217 (1983).
- ³⁵P. Bareyre, C. Bricman, M. J. Longo, G. Valladas, G. Villet, G. Bizard, J. Duchon, J. M. Fontaine, J. P. Patry, J. Seguinot, and J. Yonnet, Phys. Rev. Lett. **14**, 198 (1965).
- ³⁶P. Bareyre, C. Bricman, M. J. Longo, G. Valladas, G. Villet, G. Bizard, J. Duchon, J. M. Fontaine, J. P. Patry, J. Seguinot, and J. Yonnet, Phys. Rev. Lett. **14**, 878 (1965).
- ³⁷V. S. Bekrenev, N. F. Bondar, E. P. Fedorova-Koval, E. A. Filimonov, V. G. Gaditsky, A. I. Kovalev, S. P. Kruglov, A. A. Kulbardis, L. A. Kuz'min, I. V. Lopatin, V. E. Popov, A. N. Prokofiev, V. V. Sumachev, and V. Yu. Trautman, Nucl. Phys. **A364**, 515 (1981).
- ³⁸C. R. Cox, P. J. Duke, K. S. Heard, R. E. Hill, W. R. Holley, D. P. Jones, F. C. Shoemaker, J. J. Thresher, J. B. Warren, and J. C. Sleeman, Phys. Rev. **184**, 1453 (1969).
- ³⁹G. Bizard, F. Bonthonneau, J. Deregél, J. Duchon, J. M. Fontaine, G. Landaud, J. L. Laville, F. Lefebvres, F. Lemeilleur, J. P. Patry, H. Saur, and J. Yonnet, Nucl. Phys. **B5**, 515 (1968).
- ⁴⁰O. Chamberlain, M. J. Hansroul, C. H. Johnson, P. D. Grannis, L. E. Holloway, L. Valentin, P. R. Robrish, and H. M. Steiner, Phys. Rev. Lett. **17**, 975 (1966).
- ⁴¹J. F. Arens, O. Chamberlain, H. E. Dost, M. J. Hansroul, L. E. Holloway, C. H. Johnson, C. H. Schultz, G. Shapiro, H. M. Steiner, and D. M. Weldon, Phys. Rev. **167**, 1261 (1968).
- ⁴²R. D. Eandi, T. J. Devlin, R. W. Kenney, P. G. McManigal, and B. J. Moyer, Phys. Rev. **136**, B536 (1964).
- ⁴³D. F. Dickinson, J. A. Helland, and V. Perez-Mendez, Phys. Lett. **20**, 549 (1966).